

How Light Is Emitted by Plasmonic Metals

Jan Mertens,[†] Marie-Elena Kleemann,[†] Rohit Chikkaraddy,[†] Prineha Narang,[‡] and Jeremy J. Baumberg^{*,†}

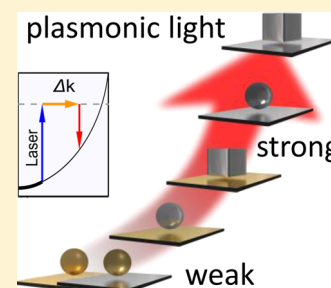
[†]NanoPhotonics Centre, Cavendish Laboratory, University of Cambridge, Cambridge CB3 0HE, United Kingdom

[‡]Faculty of Arts and Sciences, Harvard University, Cambridge, Massachusetts 02138, United States

S Supporting Information

ABSTRACT: The mechanism by which light is emitted from plasmonic metals such as gold and silver has been contentious, particularly at photon energies below direct interband transitions. Using nanoscale plasmonic cavities, blue-pumped light emission is found to directly track dark-field scattering on individual nanoconstructs. By exploiting slow atomic-scale restructuring of the nanocavity facets to spectrally tune the dominant gap plasmons, this correlation can be measured from 600 to 900 nm in gold, silver, and mixed constructs ranging from spherical to cube nanoparticles-on-mirror. We show that prompt electronic Raman scattering is responsible and confirm that “photoluminescence”, which implies phase and energy relaxation, is not the right description. Our model suggests how to maximize light emission from metals.

KEYWORDS: Plasmon, photoluminescence, nanogap, nanoparticle on mirror, Landau damping



The use of plasmonic metal nanostructures for trapping light to the nanoscale is ubiquitous for applications ranging across sensing, photocatalysis, light harvesting, near-field imaging, and photothermal therapies.^{1–6} In the dielectric gap between a pair of noble metal components, the optical field can be enhanced up to a thousand-fold at resonant wavelengths corresponding to plasmonic gap modes. Because their spectral positions can be highly sensitive to the nanoscale morphology, structural dimensions can be dynamically tracked (as in “plasmon rulers”).^{7,8} Typically the enhanced field is used for nonlinear optical processes such as surface-enhanced Raman scattering (SERS), sum-frequency conversion, or absorption.⁹ Many researchers have noticed that light can also be weakly emitted by such nanostructures, and this has been widely used to probe plasmonic structure location and identification, plasmon gap size monitoring, as well as biotagging. For individual spherical nanoparticles, the plasmon-related emission is spectrally close enough to the direct band-to-band electronic transitions to contemplate explanations based on photoluminescence.^{10–16} However, nanorods or gap plasmons can be tuned far into the infrared where such explanations cannot work.^{17–21} To date, no accepted quantitative model yet explains this phenomenon.

Here, we use a widely tunable set of nanoconstructs with $d = 1–4$ nm gaps to show light emission comes from the excitation of electrons to virtual states in the surrounding metal followed by rapid de-excitation, and is plasmon enhanced. In this way, the process closely resembles SERS from molecules in the gap but involving an intraband electronic continuum rather than discrete bond vibrations. This means that emission (unlike photoluminescence) is prompt and does not require carrier relaxation. Using light-induced sculpting of the nanoconstructs for continuous retuning of the plasmon resonances allows the

light emission to be tracked as it shifts across the visible and near-IR spectral regions. We find that silver gap plasmons emit more light than equivalent gold nanostructures and derive an analytic model that can explain the gap-size dependence based on the acceleration of the hot virtual electrons in the tightly confined plasmonic near-field gradient at the metal surface.

Explanations of metal light emission^{18,22–24} to date have included interband emission,^{25,26} local blackbody emission,^{27–29} inelastic light scattering,^{30,31} as well as intraband excitation and emission (IBEE) processes^{14,20,32,33} (related to inverse Landau damping). Recent work has emphasized the universal nature of the light emission spectrum when normalized by the dark-field scattering spectrum,³⁴ suggesting that some internal process generates broadband photons, without clearly identifying what this process is nor giving an estimate of its expected efficiency. In all mechanisms, the vertical excitation $\hbar\omega$ by photons has to be accompanied by a significant wavevector kick, Δk , to match the free electron dispersion. Identifying the origin of Δk when comparing emission from individual nanostructures has been a particular challenge because evaluating the influence of short-range surface roughness is nontrivial. Similarly, many experiments on random silver or gold colloids have been hard to draw conclusions from, due to the large diversity of random plasmonic hotspots that are averaged over.

To provide more robust reliable plasmonic nanostructures with gaps below 5 nm, we exploit the nanoparticle-on-mirror (NPoM) geometry in which colloidal nanoparticles are placed atop stiff thiol-bound self-assembled molecular (SAM) layers

Received: January 24, 2017

Revised: February 28, 2017

Published: March 7, 2017

covering a plasmonic mirror.^{35–38} Image dipoles from charge oscillations confined to the nanoparticle and to the mirror give plasmonic modes equivalent to the prototypical dimer but much more reliably and controllably. The stronger field enhancements and tighter plasmon localization also favor light emission when compared to isolated particles; we see no light emission in this spectral region from NPs on glass (though one report previously recorded similar quantum efficiencies from NP monomers and dimers²⁰). We use two sorts of nanoparticles: spherical (in practice, faceted cuboctahedron³⁹) citrate-capped Ag and Au nanoparticles (NPOMs), and Ag nanocubes (NCoMs) that are PVP capped from the synthesis protocol, placed on both Au and Ag substrates.

For Ag NCoMs, individual $D = 65$ nm Ag cubes on a BPT monolayer on a Ag mirror are alternately illuminated with white light and then continuous-wave laser radiation at 447 nm. This blue irradiation wavelength is known to provide sufficient photon energy to produce adatom drift toward the bottom nanoparticle facet, red shifting the plasmonic modes at a rate dependent on the laser power.^{40–42} For each illumination condition, a dark-field spectrum of both the scattered and emitted light is recorded (see Methods). The strong correlations in these two spectra throughout the retuning as the two observed coupled modes $j_{1,2}$ red shift (Figure 1)

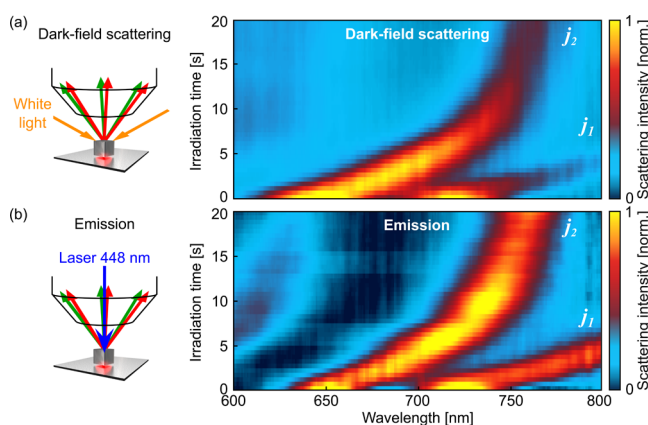


Figure 1. Correlation of dark-field and emission resonances of a single 65 nm Ag NCoM with BPT spacer. (a) Normalized color map of the dark-field scattering spectra and (b) emission spectra, as a function of irradiation time.

confirm that plasmonic resonances enhance both scattering and emission processes. Resonant scattering of high-angle incident white light matches the weak light emitted when pumped by the normally incident blue laser (when no white light is present). Emitted photon efficiencies are of order 10^{-7} . The power dependence of the emission here is always linear with blue pump intensity (in contrast to experiments where resonant pulsed excitation is used).

The precision of this match is evident in their spectral peak positions and from spectra extracted at several irradiation times (Figure 2). Only slightly less correlated are the peak amplitudes (plotted as marker size). Two different systems are shown: the Ag NCoM with a BPT spacer (Figure 2a,c) and the Ag NCoM without any additional spacer beyond its PVP capping layer (Figure 2b,d). The additional BPT spacer prevents light-induced bridging of the gap,⁴² yielding only red shifts of the resonances. However, without an additional BPT spacer both red and blue shifts of dark-field and emission resonances are

observed, explained as first an increase in cube facet width followed by the formation of a conducting bridge across the gap (schematics Figure 2e) and confirmed by theory.⁴² Comparison of the scattering (solid) and emission (dashed) spectra (Figure 2c,d) shows their similar lineshapes and line widths, implying the resonances arise from the same plasmon-enhancement process coupling light in and out. We note that slight spectral mismatches at early times are due to the faster morphological changes in the NCoM when initially laser irradiated, preventing us capturing precisely the same geometry in the successive spectra.

While mostly very similar, the strongest differences between emission and scattering are found for the late stage of conductive connection, when only a single plasmon mode can be seen (Figure 3). In this situation, despite strong DF scattering, the emission virtually disappears, even though with deeper grooves (earlier on in the irradiation) containing several plasmon modes,⁴² light emission is strong. In the final stage when metal has almost entirely replaced the dielectric layer, the plasmon field is expelled from the gap and is localized around the resulting pillar structure. The near-field decay length ($1/q$) inside this metal pillar is expanded 10-fold compared to that in the nanogap, showing this has a dramatic influence on the light emission, as expected from our model below.

Making systematic measurements on many NPOMs with both cube and sphere nanoparticles, composed of both Au and Ag, and with different gap spacers (>1500 particles for each system) allows the exploration of a large design space (Table 1). We note that the observed coupled-plasmon peak positions match very well those expected theoretically from these gap sizes. Strongest emission comes from narrow-spaced Ag cubes on Ag mirrors, which reduces as the gap size increases or either component is replaced by Au. In general, spherical nanoparticles show less emission than cubes. We also note the z-dipole orientation of these gap modes, which couples to radial polarization at high angles.^{40,41}

The model process we consider to explain the light emission can be termed as “inelastic light scattering”, which can also be described as electronic Raman scattering (ERS) though no lattice vibration is involved (discussed further in the SI). Electrons within the Fermi sea inside the metal are excited into a virtual state by the incoming plasmon-coupled photon and then de-excited back down to an empty state within the Fermi sea (Figure 4a). Because of the quadratic free-electron s-band dispersion in coinage metals, the difference in photon energy between ingoing and outgoing photons, Δ , necessarily requires a change in the momentum of the electron Δk . This is supplied by the localized spatial field distribution of the plasmon which is also responsible for coupling photons into and out of the metal. We can ignore d-bands here as the incoming and outgoing photons are detuned far from any resonant transitions between electronic states in silver (though this is not the case for gold where additional interband processes might contribute around 500 nm^{19,20}). We use a zero-temperature approximation for the Fermi distribution here, though we note ERS in the anti-Stokes background tracks the metal temperature.^{30,43} This model process is related to but differs from the Landau damping needed to explain how plasmon absorption can excite hot electrons via intraband transitions, where momentum scattering has been ascribed to defects or the nanostructure dimensions.⁴⁴ Interpreted diagrammatically (Figure 4b), the ERS process starts with photon absorption exciting an electron from below the Fermi level i to a virtual state ν , which decays to

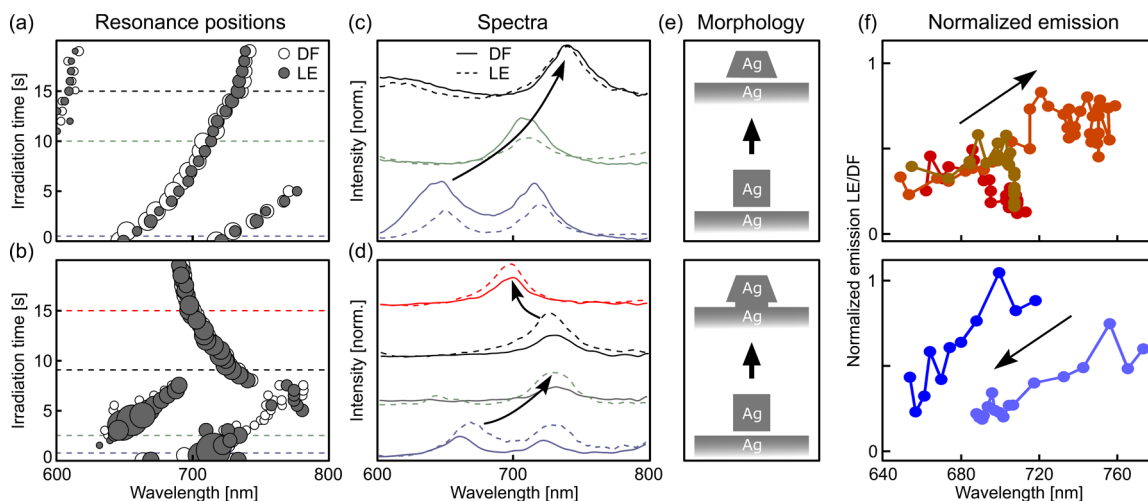


Figure 2. Correlation of dark-field (DF) scattering and light emission (LE) from individual NCoMs with (top) BPT spacer and (bottom) no additional spacer. (a,b) Extracted scattering and LE resonance positions of individual NCoMs. Marker size gives peak amplitudes. (c,d) Scattering and LE spectra at different irradiation times at color-coded horizontal lines in (a,b). (e) Schematic changes in NCoM morphology with (top) no conductive contact and (bottom) conductive contact (red) between substrate and nanoparticle. (f) Light emission amplitude as peaks spectrally shift, normalized by dark-field amplitude, for several NCoMs in red-shifting (top) or blue-shifting (bottom) regimes.

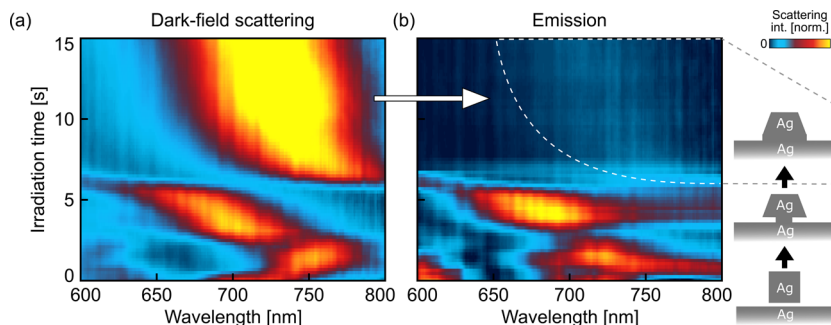


Figure 3. Normalized color maps of (a) dark-field scattering and (b) emission spectra on the same 65 nm Ag NCoM. Strong scattering continues when the gap between the Ag cube and Ag substrate is entirely filled but no emission is seen (white dashed, b).

an electron above the Fermi level f , emitting a lower energy photon. The intraband PL process is similar, except that the intermediate electron is a real state r , which is on-shell so that the energy and momentum are constrained by the dispersion relation. This additional constraint substantially reduces the phase space of intraband PL compared to ERS, making the latter process far more probable.

Either side of our plasmonic gap (taken normal to z), the field in the metal drops as $E \exp\{-qz\}$ (shown at one particular $\lambda = 720$ nm in Figure 4c, Supporting Information A) with $q = 2\varepsilon_d \operatorname{Re}\{1/\varepsilon_m(\lambda)\}/d = s/d$ for metal/dielectric permittivities $\varepsilon_{m,d}$.^{40,45} At the metal surface, electron spill-out smooths the boundary⁴⁶ over a length-scale $\delta_{QM} \sim \beta/\sqrt{\varepsilon_{\infty}^{-1}\omega_p^2 - \omega^2} \sim 0.3$ nm, using $\beta = \sqrt{3/5}v_F$ and the metal Drude parameters. Because only z momentum scattering of electrons can occur in this situation, we model the transition rate between initial i and final state f through virtual level v using Fermi's golden rule⁴⁴ with $M_{ij} = M_{iv}M_{vj}$ and (SI)

$$|M_{iv}|^2 = |\langle v|p \cdot A|i\rangle|^2 = E^2 \frac{k_{iz}^2 + q^2}{\Delta k_z^2 + q^2} \exp\{-(2\delta_{QM}\Delta k_z)^2\} \quad (1)$$

with the z -cpt momentum change $\Delta k_z = k_{fz} - k_{iz}$, and enhanced field E .⁴⁷ Integrating over all initial and final states, and the

NPoM metal volume being excited, gives the total scattering rate (SI)

$$R_{if} \propto \frac{D}{s\varepsilon_d} (1 - e^3) E_f^2 \left(\frac{l}{d}\right)^2 \quad (2)$$

with energy difference factor $e = 1 - \Delta/E_f$, nanoparticle diameter D , and critical length $l = \frac{\hbar^2 k_f}{m\Delta} = 0.34$ nm (below the quantum limit⁴⁸), for Fermi energy E_f and wavevector k_f . This allows the comparison of different metals (though E_f for Au and Ag are very similar), as well as different nanoparticle sizes, gaps, and spacers.

We can now compare the emission strength of the different constructs in Table 1. To account for the different efficiency of plasmon-induced light coupling into and out of the metal, we normalize the emission intensities with the dark-field scattering strengths (which have the same in/out-coupling efficiencies). We find that the d^{-2} dependence dominates (Figure 4d, dashed) and gives a reasonable account for each construct type. The full dependence $R_{if}(d)$ is complicated by the spectral shifts which also changes the photon energy difference Δ with gap size.

Direct comparison of different metals within the same geometry (NPoM with BPT spacer) shows some other features are also well captured by our model. The predicted enhance-

Table 1. Average Light Emission of at Least 500 NPoMs of Each Type As Listed, Normalized to the Dark-Field Scattering Peak Amplitude

	Particle	Spacer	Substrate	d_{gap} [nm]	I_{LE}/I_{DF}	
Cubes (65 nm)	Ag cube	PVP	Ag	1.5	0.54	
		PVP + BPT	Ag	2.8	0.40	
		PVP + ODT	Ag	3.8	0.22	
Spherical particles (80 nm)	Ag cube	PVP	Au	1.5	0.38	
	Ag NP	BPT	Ag	1.3	0.39	
		ODT	Ag	2.4	0.29	
	Ag NP	BPT	Au	1.3	0.28	
		PVP	Au	1.5	0.26	
		ODT	Au	2.4	0.18	
	Au NP	BPT	Ag	1.3	0.03	
		BPT	Au	1.3	0.07	

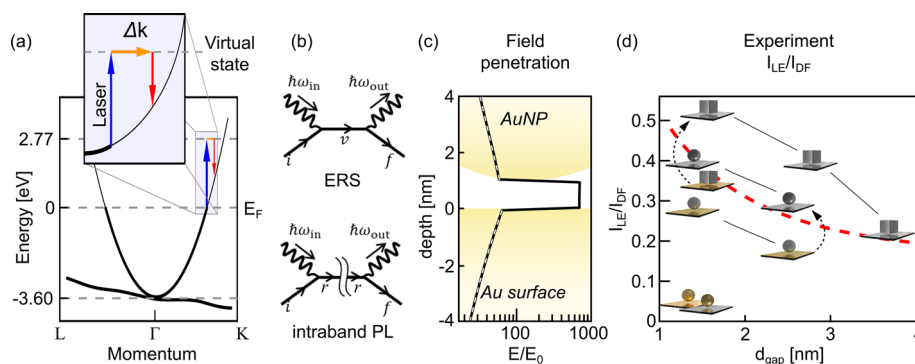


Figure 4. (a) Schematic band diagram of Ag. Laser energy of 2.77 eV is too small to excite interband transitions. Inset: ERS excited by laser, momentum Δk provided by tightly confined gap plasmon. (b) Feynman diagrams for processes of ERS (top) and intraband PL (bottom). (c) Field penetration of E_z (black line) in NPoM geometry of 1 nm gap at $\lambda = 720$ nm, exponential fit in metal (white dashed). (d) Experimentally determined intensity ratio I_{LE}/I_{DF} for cube and NP on mirror (from Table 1) with theory (red dashed).

ment from eq 2 between Au and Ag is due to $s_{Au}/s_{Ag} = 1.4$, which captures well the improvement with Ag, for instance, when a AgNP switches from a Au to a Ag substrate ($\times 1.4$) for both spheres and cubes (dashed arrows Figure 4d). On the other hand a different enhancement is seen when changing the Au to a Ag NP on a Au substrate ($\times 4$). It is thus likely that some additional effects here related to facet size and shape and oxide coating are also involved when comparing nanoparticles. This is not a problem for the flat substrates that are protected by the thiol SAMs.

Further confirmation of our ERS model comes from tracking the DF-normalized emission of single constructs while the plasmonic resonances red shift. Any model related to the spectral proximity of interband transitions (for instance, plasmon-enhanced interband PL detuned from a Lorentzian emission line) would show massive decreases in this normalized emission as it red shifts away from the Lorentzian line center, but this is not seen (Figure 2f). Instead we find that some

plasmonic modes are emissively dark (Figure 3b), depending on the precise location of the optical field, while most modes remain fully bright.

In comparison to previous models, we note that intraband photoluminescence processes (such as IBEE) require long-lived carriers to reside in high-lying states, which is highly suppressed due to their ultrashort relaxation times ($\tau_{ee} = 7$ fs for electrons, 2 fs for holes⁴⁹). By contrast, ERS operates at the same order and ultrafast speed as SERS (as shown by ref 50), and hence there are systematic correlations between the enhancements of both. Simple scaling relations for the different transition rates suggest^{47,51} that the ratio of ERS/IBEE emission $\simeq [\tau_{ee} \cdot \Delta]^{-1} \exp\{-(2\delta_{QM}q_{intra})^2\} \sim 30$ is controlled here by the large momentum transfer $q_{intra} = (\hbar\omega/2E_f)k_f \sim 3 \text{ nm}^{-1}$ needed for IBEE. Experimentally discriminating between these two ultrafast mechanisms is however currently challenging.

Although the balance of plasmonic light inside the metal (which gives ERS) and outside (which gives SERS) may change

in specific geometries, emission of light is omnipresent in all tightly confined plasmonic constructs and cannot be eliminated. We also note that because emission intensities are of similar strength at shorter wavelengths that are traditionally ascribed to interband recombination, it is probable that the same mechanism operates across the entire spectrum. We thus apply our model to several previous results in the literature, replacing the analytic dependences for the NPoM with a numerical evaluation of the overlap integrals based on full electromagnetic simulations (Supporting Information Section C) so that $R_{if} \propto \int I_{\lambda_i(\omega)} I_{\lambda_f}(\mathbf{r}) dV$, where the integral is taken only inside the metal and the intensity distributions are generated by plane wave illumination. For the case of rodlike dimers,^{52,53} we find good agreement (Supporting Information Section C) explaining the unusual rise in emission for larger gaps as a balance between less tight field localization but better in/out-coupling. When comparing dimers and monomers,²⁰ our model predicts 100-fold larger emission from the former, which suggests that in monomer emission interband PL dominates over the ERS process (Supporting Information Section D).

While the absolute value of R_{if} requires a more developed microscopic model (which is highly desirable to develop), we note our experiments imply that individual plasmonic structures are unlikely to yield emission efficiencies $>10^{-4}$ % even under further optimized conditions (to give tighter plasmon surface confinement and better radiative efficiency). Monolayer conductors such as graphene with much lower electron densities at the Fermi level will have much weaker ERS. Stimulated emission from the ERS process is different from stimulated Raman scattering because the material mode involved is an electron (fermionic) rather than a phonon (bosonic) state. Only by providing additional optical feedback at the emission energy (around the plasmon resonance) could emission be stimulated, but this would require much lower total loss than seems currently feasible.

In conclusion, we have shown that light emission from plasmonic constructs is not photoluminescence (either interband or intraband) but instead comes from photo-excitation of electrons in the metal around the nanogap to a virtual state, followed by their prompt re-emission. The essential momentum-scattering that is provided by the localized plasmon penetrating the surrounding metal surfaces can be understood in real space as rapid acceleration of the hot electron in the gradient optical field at the metal surface, resembling inverse Bremsstrahlung. We derive a general expression for the light emission strength and show how it can strongly vary according to nanoparticle shape, composition, gap size, and construct. This will open up new areas for exploration in plasmonics including light-emitting diodes or biotagging, as well as identifying crucial background emission from Purcell-enhanced quantum emitters around metals.

Methods. Sample Fabrication. Silver substrates are fabricated by direct evaporation of 10 nm Ti and 100 nm Ag onto a polished silicon wafer. Au substrates are fabricated by template stripping. A layer of 100 nm Au is evaporated on polished silicon wafers. Small silicon substrates ($10 \times 10 \text{ mm}^2$) are then glued to the Au surface using epoxy glue (EPOTEK377). The samples are left on a hot-plate for 2 h at a temperature of 150 °C to cure the epoxy glue. After cooling, the top silicon substrates are gently pushed off and Au substrates are thereby stripped with flat Au adhering to the small Si substrates.

Nanoparticles (80 nm diameter Au or Ag, citrate stabilized, BBI Scientific) or Ag nanocubes (65 nm, PVP stabilized, nanoComposix) are assembled directly on the Au or Ag substrate or on substrates covered with self-assembled monolayers (SAMs) of biphenyl-4,4'-thiol (BPT) or 1-octadecanethiol (ODT) (Sigma Aldrich, >99.8%). The SAMs are deposited by immersing the substrates for 12 h in a solution with a 1 mM concentration of the molecule in anhydrous ethanol. Unbound excess thiol is removed by rinsing the samples thoroughly with ethanol. Remaining colloidal particle solution is removed by washing samples with deionized water. The samples are dried with nitrogen.

Dark-Field and Emission Spectroscopy. A customized dark-field microscope (Olympus BX51) is used to perform dark-field white-light and emission spectroscopy of individual NPoMs in reflection geometry. For the white-light spectroscopy, incandescent light is focused with a 100× dark-field microscope objective providing high-angle illumination of up to 69° (NA = 0.93) with collection of scattered light using a numerical aperture of NA = 0.8 (Figure 1a). Scattered light is collected in confocal geometry using a 50 μm fiber as a pinhole to limit the collection area on the sample (1 μm diameter). Spectra are recorded with a cooled spectrometer (Ocean Optics QE65000) and an integration time of 300 ms.

Emission spectroscopy is realized by illuminating individual NPoMs with laser radiation using a diode laser (Coherent CUBE) with 447 nm emission wavelength, coupled to the microscope through a single-mode fiber. Collimated laser light fills the back-focal-plane of the microscope objective, thus illuminating in bright-field geometry a diffraction-limited area of 360 nm diameter on the sample. Particles are irradiated with a power of 0.2 mW, resulting in a power density of $\sim 0.8 \text{ mW}\mu\text{m}^{-2}$ (power measured after the objective at the position of the sample). The laser light is blocked using a 500 nm long-pass filter (Thorlabs) in the collection path and emitted light is recorded with the same spectrometer as for the white light spectroscopy.

Samples are placed on a motorized translation stage and each measurement step is performed as follows: first, particles are identified using a camera and their positions are saved by our algorithm.⁵¹ Particles positioned in the illumination and collection are drift compensated by automated repositioning of the NPoM in the plane and along the focus axis. White light scattering and emission spectra are then recorded subsequently: for scattering measurements, the laser is turned off. When recording emission spectra, the white light source is blocked with a shutter. After 20 scattering and emission measurements each, the focal spot is automatically shifted to the next particle on the substrate and the process is repeated. This automated process allows for measuring several hundred particles, providing a large data set for statistical analysis.

■ ASSOCIATED CONTENT

📄 Supporting Information

The Supporting Information is available free of charge on the ACS Publications website at DOI: 10.1021/acs.nanolett.7b00332.

Section A: Plasmonic field confinement in dimers. Section B: Derivation of rate of electronic Raman scattering (ERS). Section C: Comparison to literature experimental data. Section D: Comparison with intraband excitation and emission (IBEE) process. Section E:

Comparison with band-to-band transitions. Section F: Nomenclature. Section G: Emission from Au NPoM. (PDF)

AUTHOR INFORMATION

Corresponding Author

*E-mail: jjb12@cam.ac.uk

ORCID

Jeremy J. Baumberg: 0000-0002-9606-9488

Notes

The authors declare no competing financial interest.

Source data can be found at DOI link: <https://doi.org/10.17863/CAM.8417>.

ACKNOWLEDGMENTS

We thank Jacob Khurgin, Ruben Esteban, Javier Aizpurua, and Kailing Lin for enthusiastic discussions and comments. We acknowledge support from EPSRC grants EP/G060649/1, EP/L027151/1, EP/G037221/1, EPSRC NanoDTC, and ERC grant LINASS 320503. J.M. acknowledges support from the Winton Programme of the Physics of Sustainability. R.C. acknowledges support from the Dr. Manmohan Singh scholarship from St John's College, University of Cambridge.

REFERENCES

- Anker, J. N.; Hall, W. P.; Lyandres, O.; Shah, N. C.; Zhao, J.; Van Duyne, R. P. *Nat. Mater.* **2008**, *7*, 442–453.
- Brongersma, M. L.; Halas, N. J.; Nordlander, P. *Nat. Nanotechnol.* **2015**, *10*, 25–34.
- Gramotnev, D. K.; Bozhevolnyi, S. I. *Nat. Photonics* **2013**, *8*, 13–22.
- Baffou, G.; Quidant, R. *Chem. Soc. Rev.* **2014**, *43*, 3898.
- Mayer, K. M.; Hafner, J. H. *Chem. Rev.* **2011**, *111*, 3828–3857.
- Atwater, H. A.; Polman, A. *Nat. Mater.* **2010**, *9*, 205–213.
- Halas, N. J.; Lal, S.; Chang, W. S.; Link, S.; Nordlander, P. *Chem. Rev.* **2011**, *111*, 3913–3961.
- Hill, R. T.; Mock, J. J.; Hucknall, A.; Wolter, S. D.; Jokerst, N. M.; Smith, D. R.; Chilkoti, A. *ACS Nano* **2012**, *6*, 9237–9246.
- Kauranen, M.; Zayats, A. V. *Nat. Photonics* **2012**, *6*, 737–748.
- Mooradian, A. *Phys. Rev. Lett.* **1969**, *22*, 185–187.
- Boyd, G. T.; Yu, Z. H.; Shen, Y. R. *Phys. Rev. B: Condens. Matter Phys.* **1986**, *33*, 7923–7936.
- Wilcoxon, J. P.; Martin, J. E.; Parsapour, F.; Wiedenman, B.; Kelley, D. F. *J. Chem. Phys.* **1998**, *108*, 9137–9143.
- Sönnichsen, C.; Franzl, T.; Wilk, T.; von Plessen, G.; Feldmann, J.; Wilson, O.; Mulvaney, P. *Phys. Rev. Lett.* **2002**, *88*, 077402.
- Beverluis, M. R.; Bouhelier, A.; Novotny, L. *Phys. Rev. B: Condens. Matter Phys.* **2003**, *68*, 115433.
- Dulkeith, E.; Niedereichholz, T.; Klar, T. A.; Feldmann, J.; von Plessen, G.; Gittins, D. I.; Mayya, K. S.; Caruso, F. *Phys. Rev. B: Condens. Matter Phys.* **2004**, *70*, 205424.
- Shibu, E. S.; Muhammed, M. A. H.; Tsukuda, T.; Pradeep, T. *J. Phys. Chem. C* **2008**, *112*, 12168–12176.
- Mohamed, M. B.; Volkov, V.; Link, S.; El-Sayed, M. A. *Chem. Phys. Lett.* **2000**, *317*, 517–523.
- Eustis, S.; El-Sayed, M. J. *Phys. Chem. B* **2005**, *109*, 16350–16356.
- Yorulmaz, M.; Khatua, S.; Zijlstra, P.; Gaiduk, A.; Orrit, M. *Nano Lett.* **2012**, *12*, 4385–4391.
- Huang, D.; Byers, C. P.; Wang, L.-Y.; Hoggard, A.; Hoener, B.; Dominguez-Medina, S.; Chen, S.; Chang, W.-S.; Landes, C. F.; Link, S. *ACS Nano* **2015**, *9*, 7072–7079.
- Yin, T.; Dong, Z.; Jiang, L.; Zhang, L.; Hu, H.; Qiu, C.-W.; Yang, J. K. W.; Shen, Z. X. *ACS Photonics* **2016**, *3*, 979–984.
- Heritage, J. P.; Bergman, J. G.; Pinczuk, A.; Worlock, J. M. *Chem. Phys. Lett.* **1979**, *67*, 229–232.
- Huang, J.; Wang, W.; Murphy, C. J.; Cahill, D. G. *Proc. Natl. Acad. Sci. U. S. A.* **2014**, *111*, 906–911.
- Zhang, T.; Lu, G.; Shen, H.; Shi, K.; Jiang, Y.; Xu, D.; Gong, Q. *Sci. Rep.* **2014**, *4*, 3867.
- Lumdee, C.; Yun, B.; Kik, P. G. *ACS Photonics* **2014**, *1*, 1224–1230.
- Imura, K.; Nagahara, T.; Okamoto, H. *J. Am. Chem. Soc.* **2004**, *126*, 12730–12731.
- Andersen, S. K. H.; Pors, A.; Bozhevolnyi, S. I. *ACS Photonics* **2015**, *2*, 432–438.
- Tcherniak, A.; Dominguez-Medina, S.; Chang, W.-S.; Swanglap, P.; Slaughter, L. S.; Landes, C. F.; Link, S. *J. Phys. Chem. C* **2011**, *115*, 15938–15949.
- Fang, Y.; Chang, W.-S.; Willingham, B.; Swanglap, P.; Dominguez-Medina, S.; Link, S. *ACS Nano* **2012**, *6*, 7177–7184.
- Hugall, J. T.; Baumberg, J. J. *Nano Lett.* **2015**, *15*, 2600–2604.
- Otto, A.; Akemann, W.; Pucci, A. *Isr. J. Chem.* **2006**, *46*, 307–315.
- Lin, K.-Q.; Yi, J.; Hu, S.; Sun, J.-J.; Zheng, J.-T.; Wang, X.; Ren, B. *ACS Photonics* **2016**, *3*, 1248–1255.
- Haug, T.; Klemm, P.; Bange, S.; Lupton, J. M. *Phys. Rev. Lett.* **2015**, *115*, 067403.
- Hu, H.; Duan, H.; Yang, J. K. W.; Shen, Z. X. *ACS Nano* **2012**, *6*, 10147–10155.
- Benz, F.; Tserkezis, C.; Herrmann, L. O.; de Nijs, B.; Sanders, A.; Sigle, D. O.; Pukenas, L.; Evans, S. D.; Aizpurua, J.; Baumberg, J. J. *Nano Lett.* **2015**, *15*, 669–674.
- Mock, J. J.; Hill, R. T.; Degiron, A.; Zauscher, S.; Chilkoti, A.; Smith, D. R. *Nano Lett.* **2008**, *8*, 2245–2252.
- Ciraci, C.; Hill, R. T.; Mock, J. J.; Urzhumov, Y.; Fernandez-Dominguez, A. I.; Maier, S. a.; Pendry, J. B.; Chilkoti, A.; Smith, D. R. *Science* **2012**, *337*, 1072–1074.
- Mertens, J.; Eiden, A. L.; Sigle, D. O.; Huang, F.; Lombardo, A.; Sun, Z.; Sundaram, R. S.; Colli, A.; Tserkezis, C.; Aizpurua, J.; Milana, S.; Ferrari, A. C.; Baumberg, J. J. *Nano Lett.* **2013**, *13*, 5033–5038.
- Benz, F.; Chikkaraddy, R.; Salmon, A.; Ohadi, H.; de Nijs, B.; Mertens, J.; Carnegie, C.; Bowman, R. W.; Baumberg, J. J. *J. Phys. Chem. Lett.* **2016**, *7*, 2264–2269.
- Sigle, D. O.; Mertens, J.; Herrmann, L. O.; Bowman, R. W.; Ithurria, S.; Dubertret, B.; Shi, Y.; Yang, H. Y.; Tserkezis, C.; Aizpurua, J.; Baumberg, J. J. *ACS Nano* **2015**, *9*, 825–830.
- Tserkezis, C.; Esteban, R.; Sigle, D. O.; Mertens, J.; Herrmann, L. O.; Baumberg, J. J.; Aizpurua, J. *Phys. Rev. A: At., Mol., Opt. Phys.* **2015**, *92*, 053811.
- Mertens, J.; Demetriadou, A.; Bowman, R. W.; Benz, F.; Kleemann, M.-E.; Tserkezis, C.; Shi, Y.; Yang, H. Y.; Hess, O.; Aizpurua, J.; Baumberg, J. J. *Nano Lett.* **2016**, *16*, 5605.
- Ward, D. R.; Corley, D. A.; Tour, J. M.; Natelson, D. *Nat. Nanotechnol.* **2011**, *6*, 33–38.
- Khurgin, J. B. *Faraday Discuss.* **2015**, *178*, 109–122.
- Benz, F.; de Nijs, B.; Tserkezis, C.; Chikkaraddy, R.; Sigle, D. O.; Pukenas, L.; Evans, S. D.; Aizpurua, J.; Baumberg, J. J. *Opt. Express* **2015**, *23*, 33255.
- Luo, Y.; Fernandez-Dominguez, A. I.; Wiener, A.; Maier, S. A.; Pendry, J. B. *Phys. Rev. Lett.* **2013**, *111*, 185–187.
- Khurgin, J. B.; Sun, G. In *Quantum Plasmonics*; Bozhevolnyi, S. I., Martin-Moreno, L., Garcia-Vidal, F., Eds.; Springer, 2017; pp 302–320.
- Savage, K. J.; Hawkeye, M. M.; Esteban, R.; Borisov, A. G.; Aizpurua, J.; Baumberg, J. J. *Nature* **2012**, *491*, 574–577.
- Brown, A. M.; Sundararaman, R.; Narang, P.; Goddard, W. A.; Atwater, H. A. *ACS Nano* **2016**, *10*, 957–966.
- Varnavski, O. P.; Mohamed, M. B.; El-Sayed, M. A.; Goodson, T. J. *Phys. Chem. B* **2003**, *107*, 3101–3104.
- Khurgin, J. B.; Sun, G.; Friedman, L. R.; Soref, R. A. *J. Appl. Phys.* **1995**, *78*, 7398.

(52) Sivun, D.; Vidal, C.; Munkhbat, B.; Arnold, N.; Klar, T. A.; Hrelescu, C. *Nano Lett.* **2016**, *16*, 7203–7209.

(53) de Nijs, B.; Bowman, R. W.; Herrmann, L. O.; Benz, F.; Barrow, S. J.; Mertens, J.; Sigle, D. O.; Chikkaraddy, R.; Eiden, A.; Ferrari, A.; Scherman, O. A.; Baumberg, J. J. *Faraday Discuss.* **2015**, *178*, 185–193.